Geophysical Research Letters

RESEARCH LETTER
10.1029/2025GL119264

MOS and RREA Processes in Thunderclouds: Intensities and Spectral Shapes

Ashot Chilingarian[1] and **Mary Zazyan**[1]

[1]A I Alikhanyan National Lab (Yerevan Physics Institute), Yerevan, Armenia

Key Points:

- We demonstrate how a relatively mild flux enhancement process in thunderclouds shifts to an abrupt increase mode
- We provide a practical method to infer thundercloud electric-field evolution from Thunderstorm Ground Enhancements (TGEs)
- We demonstrate that a small Atmospheric Electric Field (AEF) variance can lead to flux changes in the Relativistic Runaway Electron Avalanche (RREA) by an order of magnitude

Correspondence to:
A. Chilingarian,
chili@aragats.am

Citation:
Chilingarian, A., & Zazyan, M. (2025). MOS and RREA processes in thunderclouds: Intensities and spectral shapes. *Geophysical Research Letters*, *52*, e2025GL119264. https://doi.org/10.1029/2025GL119264

Received 17 SEP 2025
Accepted 25 NOV 2025

Author Contributions:
Conceptualization: Ashot Chilingarian
Data curation: Mary Zazyan
Formal analysis: Mary Zazyan
Methodology: Ashot Chilingarian
Supervision: Ashot Chilingarian
Validation: Mary Zazyan
Visualization: Mary Zazyan
Writing – original draft: Ashot Chilingarian

Abstract The Relativistic Runaway Electron Avalanche (RREA) is the primary mechanism for enhancing atmospheric electron and gamma-ray fluxes when the electric field exceeds a density-dependent threshold. Another, non-threshold process—Modification of the Electron Energy Spectrum (MOS)—occurs when subcritical fields energize ambient electrons, shifting their spectrum to higher energies and increasing bremsstrahlung probability. MOS becomes dominant at high energies, where the RREA flux rapidly decreases, explaining the persistent detections of gamma rays above 50–60 MeV. We simulate gamma-ray yield over a wide range of Atmospheric Electric Field (AEF) to delineate MOS and RREA regimes and quantify spectral evolution with field strength. Experimental data from two Thunderstorm Ground Enhancements (TGEs) observed on 2 October 2024, are analyzed. By matching the exponential growth of measured count rates to modeled RREA yield, we derive the temporal evolution of the AEF during both TGEs, revealing the rate and magnitude of field strengthening that drive particle bursts and bridge the MOS–RREA transition in natural thunderstorms.

Plain Language Summary Thunderstorms can act like natural particle accelerators in the air above the surface. When the electric field inside a storm becomes strong, it can energize some of the electrons that constantly rain down from space (cosmic rays). We show that two mechanisms are at work. In MOS (Modification of the Electron Energy Spectrum), moderate fields gently push existing electrons to higher energies, creating more gamma rays. In RREA, when the field exceeds a critical level, it triggers a chain reaction that multiplies electrons and gamma rays significantly. Using detailed computer simulations and measurements from our high-altitude station on Mount Aragats (Armenia), we map how gamma-ray intensity increases as the field strengthens. These results help translate particle measurements into practical information about changing storm electricity. This can improve lightning forecasting, inform aviation about radiation hot spots along flight routes, and guide the safe operation of ground instruments during severe weather.

1. Introduction

Thundercloud charges and atmospheric electric fields (AEFs) are among the most difficult phenomena to measure and simulate. The connection between cloud electrification and particle fluxes moving through thunderclouds remains a key focus in high-energy physics in the atmosphere research. Interactions with solar radiation, cosmic ray fluxes, atmospheric discharges, and winds greatly affect the behavior of AEF. Electric charge in the atmosphere can be carried by hydrometeors and neutralized by atmospheric discharges. Therefore, gaining insight into the electrodynamics of charged clouds is challenging. Overall, very few direct measurements of AEFs in thunderclouds have been reported (Stolzenburg et al., 1994, 2007). To date, no simultaneous measurements of particle fluxes and the AEFs that produce them have been conducted (Eack & Beasley, 2015). As a result, a phenomenological approach is used to investigate the relationships between emerging electric fields and particle fluxes. In this paper, we infer electric field dynamics from thunderstorm ground enhancement (TGE, Chilingarian et al., 2010, 2011) time series, building on our method of combining TGE measurements with CORSIKA simulations to determine AEF evolution during thunderstorms (Chilingarian et al., 2022).

Charged particles entering AEFs undergo acceleration or deceleration, emitting bremsstrahlung gamma rays in both cases. If the electric field strength is high enough, a relativistic runaway electron avalanche (RREA, Gurevich & Milikh, 1992) is initiated. Millions of electrons, gamma rays, and neutrons reach the Earth's surface, creating large particle bursts (see citations to original publications in review papers (Chilingarian, 2024; Chilingarian, Williams, et al., 2025). When the AEF strength is below the threshold energy required to start the avalanche—which depends on air density or altitude in the atmosphere—bremsstrahlung still increases, leading to

additional gamma-ray flux reaching the surface. This process is known as the modification of the electrons' energy spectrum (MOS; Chilingarian et al., 2012).

By simulating and analyzing RREA particle intensities and yields from CORSIKA simulations at different AEF strengths, and comparing them with measured time series of particle detector count rates, we clearly observe the transition from MOS to RREA as the AEF increases. From simulations across a broad range of AEFs covering both MOS and RREA domains, and by observing large TGE events, we develop a methodology to determine AEF dynamics during strong TGEs. To our knowledge, this is the first integrated use of count-growth and CORSIKA responses to derive AEF evolution during TGEs.

2. Method: CORSIKA Simulations of MOS and RREA Processes

To examine the relationship between MOS and RREA processes, we conducted simulation trials using free-electron seeds from the ambient cosmic-ray population across a wide range of AEF strengths, from well below the RREA threshold to fields that exceed it. This method ensures the separation of the two gamma-ray flux enhancement mechanisms. We used the CORSIKA 7.7550 simulation code (Heck et al., 1998), incorporating the EGS4 package for electromagnetic interactions. The CORSIKA option was enabled to monitor RREA development in the presence of vertically aligned electric fields. An electric field was applied above the high-altitude Aragats station at (3,300–5,300 m a.s.l.). The seed electron spectrum was defined in the energy range of $E_{seed} = 1$–300 MeV, following a power-law distribution with an index of -1.25, as estimated from secondary cosmic ray spectra using the EXPACS web calculator (Sato, 2016). Also, fixed seed electron energies of 100 and 300 MeV were tested. Simulations were conducted for electric field strengths ranging from 0.4 to 2.2 kV/cm. For each Ez value, we recorded the number of electrons and photons at 200 m intervals during propagation. Energy cuts for secondary particles were 0.3 GeV (hadrons), 0.01 GeV (muons), 0.00005 GeV (electrons), and 0.00005 GeV (photons). No thinning or curved options were used. The standard US atmosphere option was implemented. The zenith angle was selected randomly within the range's lower and upper bounds, ensuring equal particle fluxes from all sky solid angles and corresponding to a flat horizontal detector setup. In Figure 1, the simulation results for an AEF of 1.2 kV/cm are displayed.

Figure 1 shows that the MOS process can increase particle flux when AEF is well below the RREA threshold. Also, we see that there is no energy limit for MOS gamma rays. For 100 MeV seeds, the maximum energy is 100 MeV, and for 300 MeV seeds, it is 300 MeV. These represent extreme cases where a seed electron transfers all its energy to the bremsstrahlung gamma ray.

In Table 1, we demonstrate how particle fluxes depend on the electric field strength they pass through. We show the gamma-ray yield for 50 keV and 5 MeV. The 5 MeV is the energy threshold of the particle detectors at Aragats station. Up to 1.6 kV/cm, we see a steady increase, which we attribute to the MOS effect, a shift of the electron energy spectrum to higher values that boosts bremsstrahlung probability. At 1.8 kV/cm, the runaway threshold is surpassed, and the gamma-ray flux sharply increases. Above the threshold, it is difficult to measure the "pure" MOS process; however, we can estimate its contribution by extrapolating the fit from 0.4 to 1.6 kV/cm to higher values. This method helps us to overcome the overwhelming flux of RREA gamma rays.

In Figure 2, we illustrate how the gamma ray yield from the MOS process gradually increases with AEF and then surges due to RREA starting at approximately 1.7 kV/cm. The yield becomes very sensitive to AEF once the field enters the runaway regime. Between 1.6 and 2.2 kV/cm, the exponent index (the slope of ln n vs. Ez) is about $g = 16$ (kV/cm)$^{-1}$, compared to 0.54 (kV/cm)$^{-1}$ for MOS. A large index indicates a very steep response: small increases in Ez lead to order-of-magnitude changes in gamma yield, which is characteristic of the avalanche regime and a signature of avalanche multiplication.

In Table 2, we show MOS and RREA contributions to the increased gamma-ray flux. The MOS exponent increases gradually, and when extrapolated, it contributes modestly at 1.8 kV/cm (16.9%) and becomes negligible at 2.0 kV/cm (0.54%) for energies above 50 keV. For energies above 5 MeV, MOS's share at AEF of 1.8 is significant at 45.6%, but it also drops to 2.6% at 2.0 kV/cm and to 0.1% at 2.2 kV/cm. The sharp rise beyond approximately 1.6 kV/cm results from RREA; the avalanche multiplies particle numbers so rapidly that MOS becomes insignificant. In the next section, we will compare model calculations summarized by the f (MOS) and g (RREA) exponent indices with the time series of large TGE recorded at Aragats on 2 October 2024.

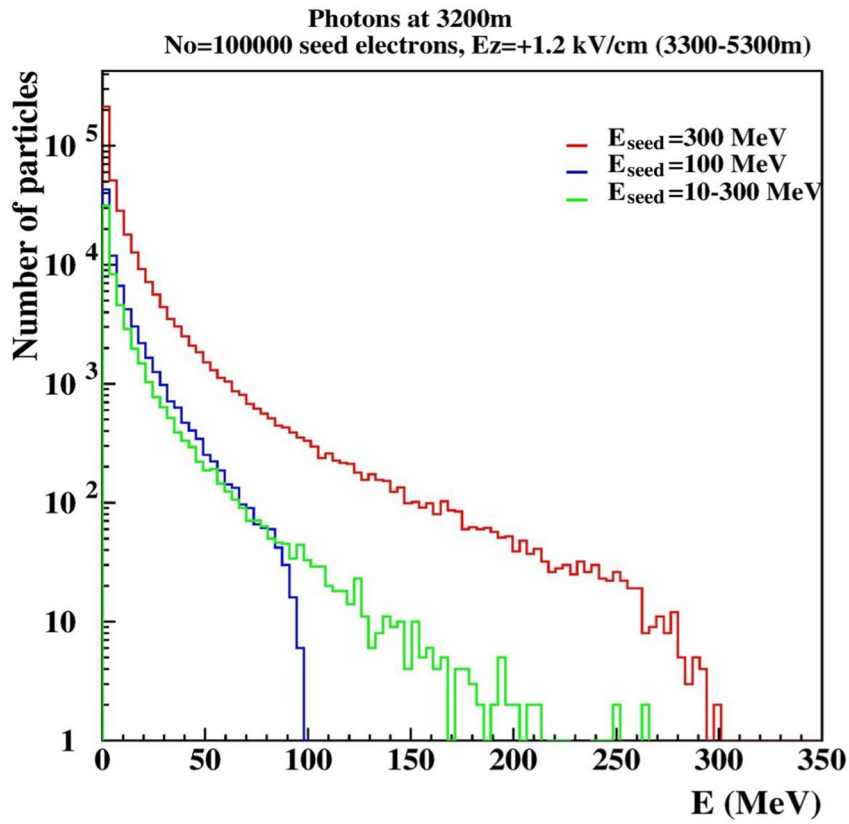

Figure 1. Energy spectrum (in arbitrary units)of gamma rays originating from seed electrons in atmospheric electric fields. The blue curve represents 100 MeV seeds, the red curve 300 MeV seeds, and the green curve 10–100 MeV seeds. Number of seed electrons: 100,000. Observation level: 3,200 m. AEF of 1.2 kV/cm applied at altitudes between 3,300 and 5,300 m.

3. Results 1: Analysis of 2-Stage TGE Occurred on 2 October 2024

Just after midnight on 2 October 2024, from 00:41:40 to 00:43:36, particle detectors on Aragats recorded a significant increase in particle flux count rates, as shown in Figure 3 (blue curve). During the deep negative near-surface electric field (NSEF, black curve), the count rate of a 1-cm-thick, 1 m^2 plastic scintillator of the STAND1 network (located on the roof of the GAMMA calorimeter) shows two large increases. The first, lasting about

Table 1
Number of Particles (>5 MeV and >50 KeV) per Seed Electron

Ez kV/cm	Ne− (>50 KeV)	Ne+ (>50 KeV)	Nγ (>50 KeV)	Ne− (>5 MeV)	Ne+ (>5 MeV)	Nγ (>5 MeV)
0.4	0.012	0.004	0.276	0.008	0.003	0.118
0.6	0.014	0.004	0.313	0.008	0.004	0.132
0.8	0.016	0.005	0.365	0.010	0.004	0.149
1.0	0.019	0.006	0.442	0.012	0.004	0.174
1.2	0.023	0.006	0.570	0.014	0.005	0.207
1.4	0.030	0.007	0.787	0.017	0.006	0.262
1.6	0.042	0.009	1.356	0.024	0.006	0.370
1.8	0.101	0.014	6.088	0.041	0.009	0.862
2.0	2.39	0.12	233.18	0.47	0.04	18.21
2.2	180.21	5.3	9,091.19	62.02	1.72	741.62

Note. Number of seed electrons: 100,000. Index of electron energy spectrum $\gamma = -1.25$. Observation level: 3,200 m. Electric field introduced at 3,300–5,300 m.

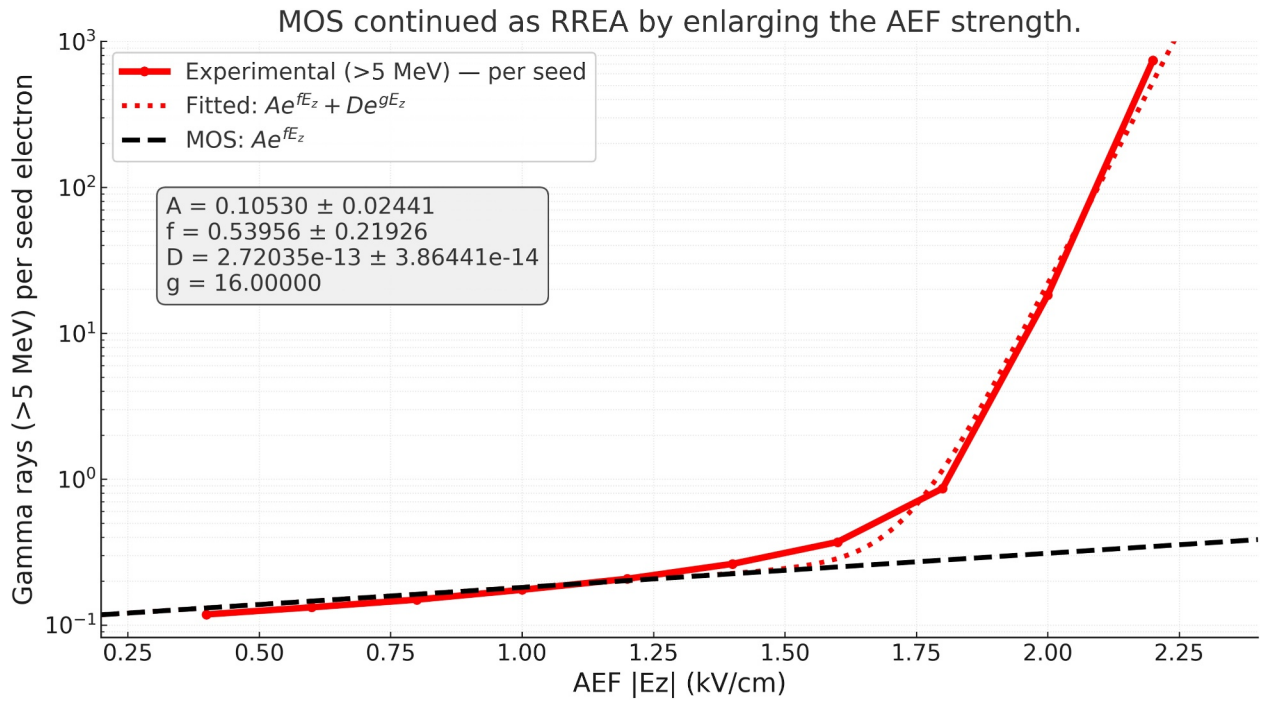

Figure 2. The increase in gamma-ray yield due to MOS/Relativistic Runaway Electron Avalanche processes. Red curves: two-exponential fit across 0.4–2.2 kV/cm. Black curve - MOS yield extrapolated to 2.2 kV/cm.

2 min, gradually declines after reaching a maximum of 423%. The second, lasting about 25 s, was abruptly halted at its peak flux—nine times the background level—by a cloud-ground (-CG) lightning strike that disrupts the local electric field and returns particle flux to the background level. Between two TGEs, the NSEF maintains the particle flux at a high level, roughly twice the background. Subsequently, we observe a sharp increase in the second TGE to 459% (relative to the already enhanced flux of 1,000/m^2 s at the beginning of the second count rate rise) within 25 s (approximately 894% if we consider the "genuine" background level of about 500/m^2 s as baseline).

In Figure 4, we show a 1-s time series illustrating the different growth rates of TGE. TGE1 starts at 00:41:00 and gradually ends at 00:43:12, showing a 423% increase over 2 min; TGE2 begins at 00:43:20 and ends with a lightning flash at 00:43:45. The increase relative to the background measured before the TGE1 event was 894%, and relative to the start of TGE2 (≈1,000) was 459%. To relate growth speeds with the corresponding AEF enhancements, we use CORSIKA simulations presented in Figure 2. Building on these two TGEs, we develop a method to infer the AEF evolution during TGEs by connecting measurements of particle fluxes with CORSIKA simulations. As mentioned earlier, AEF evolution during TGEs has never been experimentally measured, and our goal is to indirectly determine it by combining measurements and CORSIKA simulations. We call this approach

Table 2
MOS Versus Relativistic Runaway Electron Avalanche Shares (First Exponent for MOS) at Ez = 1.8, 2.0, and 2.2 kV/Cm

Band	Ez (kV/cm)	MOS (first exponent)	Total	MOS share	RREA share
>50 keV	1.8	1.022	6.088	16.8%	83.2%
>50 keV	2.0	1.249	233.180	0.5%	99.5%
>50 keV	2.2	1.525	9,091.190	0.0%	100.0%
>5 MeV	1.8	0.393	0.862	45.6%	54.4%
>5 MeV	2.0	0.472	18.210	2.6%	97.4%
>5 MeV	2.2	0.568	741.620	0.1%	99.9%

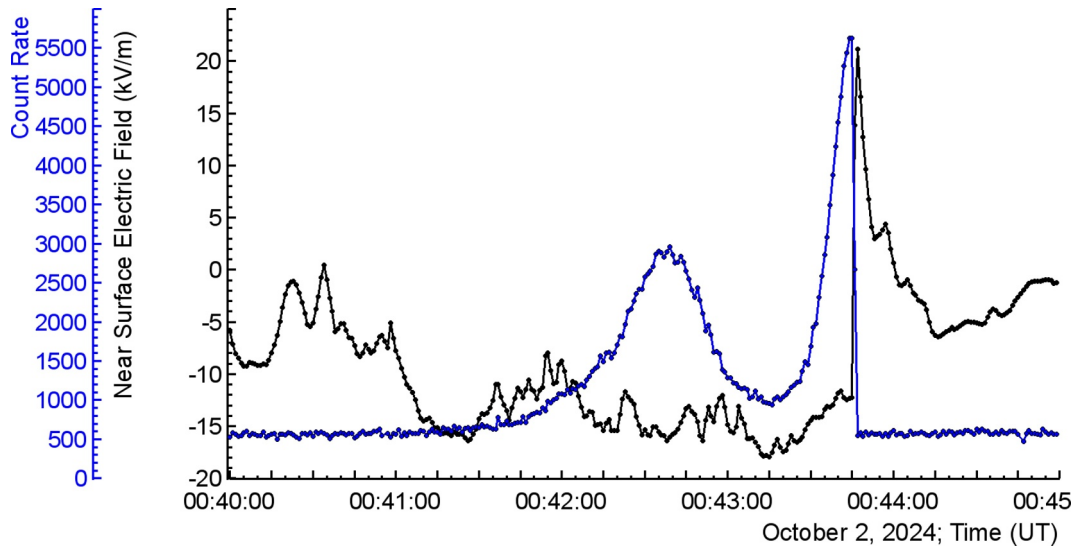

Figure 3. Two-stage thunderstorm ground enhancement occurred at a negative near-surface electric field. Black–NSEF measured by EFM-100 electric mill, blue–1-s time series of count rate from a 1-cm thick, 1-m^2 area plastic scintillator of the STAND1 network.

Monte-Carlo statistical inference, which was first used for event-by-event classification of primary nuclei in the MAKET (Chilingarian et al., 2004) and KASCADE (Antoni et al., 2002) experiments.

4. Results 2: AEF Evolution During TGEs

Our method utilizes synchronized streams of CORSIKA simulations for the RREA processes, complemented by experimental data on increased particle fluxes measured at Earth's surface.

Simulation channel: from CORSIKA simulations, we obtain the yield per seed electron, Isim (Ez), for gamma rays above 5 MeV (Table 1, last column). In the MOS domain, the growth with field is gradual; when the field reaches the runaway regime (1.6–2.2 kV cm^{-1}), the gamma-ray yield increases exponentially.

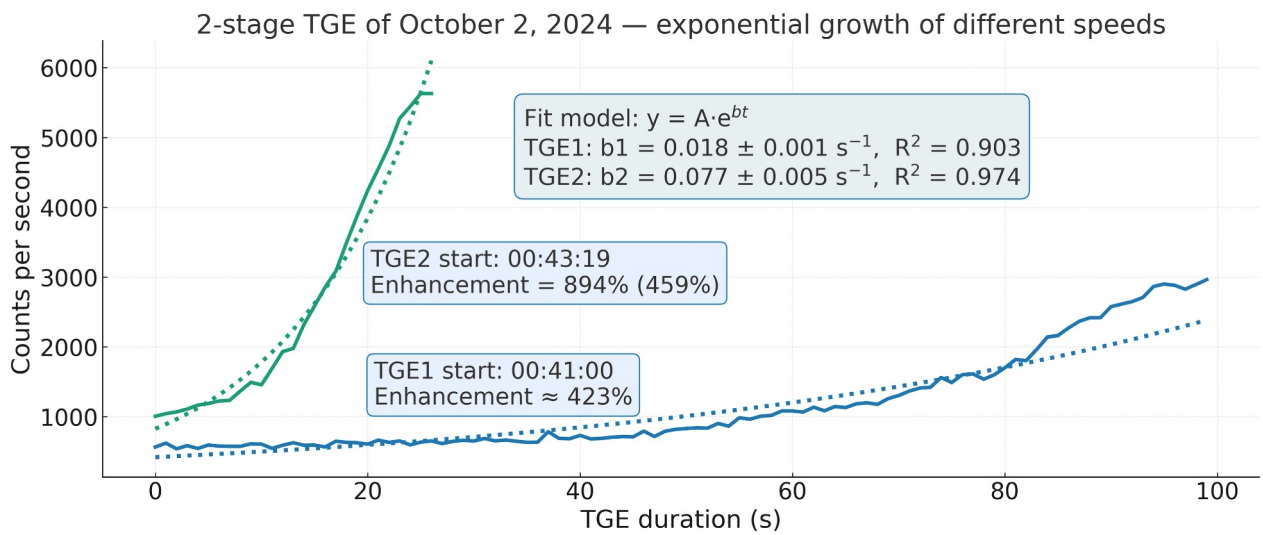

Figure 4. Time series of two Thunderstorm Ground Enhancements on 2 Oct 2024, sampled at 1-s resolution. Solid curves show measured count rates: TGE1 (blue) and TGE2 (green). Dotted curves are exponential fits with indices $b = 0.018$ s^{-1} for TGE1 and $b = 0.077$ s^{-1} for TGE2. Start times (UTC) and total enhancements are annotated near each curve.

$$I_{sim}(E_z) \approx D\, e^{gEz}, E_z \in [1.6, 2.2]\ \text{kV cm}^{-1}, g \approx 16, E_z \approx E_0 + \alpha t. \quad (1)$$

Simulated count rate will look as

$$N_{sim}\left(E_z(t)\right) \approx C\, I_{sim}\, e^{g\alpha t}, C = DSK\, e^{gE0}, \quad (2)$$

where exponent index g is the slope of $\ln I_{sim}$ versus Ez in that AEF runaway range, S is the seed electron rate, and K is the detector response function. For short TGE intervals, we approximate the field as linear: $Ez(t) \approx E_0 + \alpha * t$, where E_0 is the threshold level for RREA (2.2–1.6 kV/cm for 3,000–5,000 m, Chilingarian, Hovhannisyan, & Zazyan, 2025), and α is the rate of change of Ez. We assume that the coefficients S, K are effectively constant over the short window of fit (Chilingarian et al., 2022).

Data channel: from the 1-s time series, we select lightning-free rising segments for the two TGEs. Each segment is well fit by

$$N_{TGE}(t) = A\, e^{bt}, \quad (3)$$

where $b1 \approx 0.017\ s^{-1}$ for TGE1 (longer, slower TGE) and $b2 \approx 0.077\ s^{-1}$ for TGE2 (short, faster TGE).

Bridge: now we have two exponents describing the count rate evolution for both simulated and experimental events, and we can assume that the measured counts are proportional to the simulated yield, and readily obtain:

$$g\alpha = b. \quad (4)$$

Then we obtain an estimate of the AEF change during the enhancing phase of TGE:

$$\Delta E_z \approx b/g\ \Delta t. \quad (5)$$

Finally, after applying g and $b1$, $b2$ from the fits shown in Figures 2 and 4, we obtain absolute field increases (AEF is negative, thus the field becomes more negative) and linear coefficients of field rise $\alpha = b/g$:

$$\text{TGE1 (00:41:00–00:42:39): } \Delta Ez \approx 0.1084 \pm 0.0036\ \text{kV/cm}, \alpha 1 = 1.1 \pm 0.036\ \text{V/cm s}.$$

$$\text{TGE2 (00:43:19–00:43:45): } \Delta Ez \approx 0.1249 \pm 0.0041\ \text{kV/cm}, \alpha 2 = 4.803 \pm 0.157\ \text{V/cm s}.$$

These values agree with the rounded values displayed in Figure 4.

5. Conclusions

We demonstrate MOS and RREA processes within a single simulation trial. Once AEF surpasses the RREA threshold, seed electrons initiate a runaway avalanche, which appears on the Earth's surface as TGE. The primary effect is not just per-electron energy gain, but the rapid exponential increase in the number of relativistic electrons and gamma rays; this multiplication accounts for the steep exponent seen when fitting particle growth as the simulated AEF enlarges from 1.6 to 2.2 kV/cm (Figure 2). This approach aligns with the MOS concept introduced by Chilingarian et al. (2012). In sub-critical fields, the MOS mechanism was the leading explanation for gamma-ray brightening observed during balloon and aircraft measurements (Kelley et al., 2015; Ostgaard et al., 2019).

We connect the RREA-modeled data with the largest TGE observed on Aragats over the past 2 years (2 October 2024, Figure 3). Using explicit model assumptions, we perform a joint analysis of simulation (CORSIKA) and experimental (TGE) data and derive an equation linking both, thereby providing insight into the dynamics of the AEF during RREA. The local bridge allows us to infer the field-ramp rate $\alpha = b/g$ and the net field change $\Delta Ez = (b/g)\ \Delta t$ within short, lightning-free particle growth windows.

To our knowledge, this is the first attempt to infer time-resolved AEF evolution above the RREA threshold directly from simulations calibrated to ground measurements. Direct in-cloud measurements of AEF in this

regime are not yet available, so our approach provides a practical path to quantify AEF dynamics during TGEs. It can be used for observing gamma-ray glows seen on Japan's eastern coast (Tsuchiya et al., 2007; Wada et al., 2021) and during the ALOFT mission (Marisaldi et al., 2024). In both cases, the RREA ended well away from the detectors, so only gamma rays are detected, as electrons were attenuated.

The large g in Figure 2 and the larger $b2$ (relative to $b1$) in Figure 4 illustrate how AEF changes drive order-of-magnitude variations in counts in both simulations and experiment. For the 2 October 2024 event we find ΔEz (TGE1) = 0.108 ± 0.004 kV/cm and ΔEz (TGE2) = 0.125 ± 0.004 kV/cm, corresponding to $\alpha 1 = 1.095 \pm 0.036$ and $\alpha 2 = 4.803 \pm 0.157$ V cm^{-1} s^{-1} Consistent with balloon observations in New Mexico (Stolzenburg et al., 2007), we estimate that the AEF increased from ∼2.07 to ∼2.20 kV/cm over 25 s before lightning ended TGE2.

Limitations and outlook. Our inferences rely on short windows where the field is approximately linear in time, on proportionality between counts and simulated yield with slowly varying seed and detector factors, and on using a local simulation slope g in the RREA band. These assumptions define the main sources of statistical and systematic uncertainty. Future work should refine g (Ez, altitude), extend the analysis to multi-station TGEs, and co-analyze with lightning mapping and in-cloud probes as such data becomes available. Despite these caveats, our results demonstrate that AEF dynamics in the RREA domain can be constrained in the absence of direct measurements, laying the groundwork for routine, simulation-assisted AEF diagnostics during TGEs.

Abbreviations

RREA	The Relativistic Runaway Electron Avalanche
MOS	Modification of the Electron Energy Spectrum
AEF	Atmospheric Electric Field
NSEF	Near-surface Electric Field
TGEs	Thunderstorm Ground Enhancements

Definitions, and Model Assumptions

- I_{sim} (Ez): simulated particle yield at detector level per seed electron as a function of the vertical field Ez (kV/cm) used in simulations.
- N_{sim} (Ez): expected simulated particle count rate per second per m^2 as a function of the vertical field Ez (kV/cm).
- N_{TGE}(t)–1-s time series of count rates measured at the enhancing phase of TGE of 2 October 2024.
- Ez–the atmospheric electric field, remaining negative (according to the atmospheric electricity notion) during TGEs of 2 October 2024.
- g: exponent index, defined as the slope of simulated lnN_{sim} versus Ez in the chosen high-field band (1.8–2.2 kV/cm).
- $b1$ and $b2$: time exponents fitted by the rising phase of the TGE time series (N_{TGE}(t)).
- α: AEF increase per second; α = dEz/dt kV·cm^{-1} s^{-1}.
- R: TGE enhancement factor, ratio of end to start counts.
- S: electron seed rate at the start of the lower dipole (taken constant over the TGE time).
- K: detector response function, constant over the TGE time.
- The electric field Ez increases approximately linearly during the enhancing phase of TGE: Ez(t) ≈ $E_0 + \alpha$ * t, where E_0 is the initial field strength at the start of RREA, and α is the AEF increase per second (kV/cm per second).
- The AEF-domain curve is locally exponential, so the exponential index g is approximately constant over the TGE growing phase.
- During each short TGE rising window, the field increases smoothly, so exponential indecies $b1$ and $b2$ are meaningful.
- Most of the particles detected during TGE are gamma rays.

- The energy dependence of the detector response function K can be neglected for the energy range (7–50 MeV).
- The simulation output I_{sim} (Ez) is computed for the same energy band (e.g., >5 MeV), altitude, and geometry used in the data analysis.

Conflict of Interest

The authors declare no conflicts of interest relevant to this study.

Data Availability Statement

The TGE archive till 2024 is freely available in graphical and numerical formats from the Mendelay site at doi: 10.17632/8gtdbch59z (Chilingarian et al., 2024). Data archive on CORSIKA simulations (MOS and RREA development in the atmosphere) is available at the link: http://crd.yerphi.am/CORSIKA_Simulations.

Acknowledgments
None.

References

Antoni, T., Apel, W., Badea, F., et al. (2002). A non-parametric approach to infer the energy spectrum and the mass composition of cosmic rays. *The Astrophysical Journal*, *662*(2), 892.

Chilingarian, A. (2024). Extensive air showers and atmospheric electric fields. Synergy of space and atmospheric particle accelerators. *Advances in Space Research*, *74*(9), 4388–4402. https://doi.org/10.1016/j.asr.2024.03.013

Chilingarian, A., Daryan, A., Arakelyan, K., Hovhannisyan, A., Mailyan, B., Melkumyan, L., et al. (2010). Ground-based observations of thunderstorm-correlated fluxes of high-energy electrons, gamma rays, and neutrons. *Physics Review D*, *82*(4), 043009. https://doi.org/10.1103/PhysRevD.82.043009

Chilingarian, A., Gharagyozyan, G., Hovsepyan, Ghazaryan, S., Melkumyan, L., & Vardanyan, A. (2004). Light and Heavy Cosmic Ray Mass Group energy Spectra as measured by the MAKET-ANI detector. *The Astrophysical Journal*, *603*(1), L29–L32. https://doi.org/10.1086/383086

Chilingarian, A., Hovhannisyan, L., & Zazyan, M. (2025). Threshold atmospheric electric fields for initiating relativistic runaway electron avalanches: Theoretical estimates and CORSIKA simulations. *EGUSPHERE-2025-4153*. https://editor.copernicus.org/EGUsphere/ms-records/egusphere-2025-4153

Chilingarian, A., Hovsepyan, G., & Hovhannisyan, A. (2011). Particle bursts from thunderclouds: Natural particle accelerators above our heads. *Physics Review D*, *83*(6), 062001. https://doi.org/10.1103/PhysRevD.83.062001

Chilingarian, A., Hovsepyan, G., Karapetyan, T., Sargsyan, B., & Zazyan, M. (2022). Development of the relativistic runaway avalanches in the lower atmosphere above mountain altitudes. *EPL*, *139*(5), 50001. https://doi.org/10.1209/0295-5075/ac8763

Chilingarian, A., Karapetyan, T., Sargsyan, B., Aslanyan, D., & Chilingaryan, S. (2024). Dataset on extreme thunderstorm ground enhancements registered on Aragats in 2023. *Data in Brief*, *54*, 110554. https://doi.org/10.1016/j.dib.2024.110554

Chilingarian, A., Mailyan, B., & Vanyan, L. (2012). Recovering of the energy spectra of electrons and gamma rays coming from the thunderclouds. *Atmospheric Research*, *114–115*, 1–16. https://doi.org/10.1016/j.atmosres.2012.05.008

Chilingarian, A., Williams, E., Hovsepyan, G., & Mkrtchyan, H. (2025). Why Schonland failed in his search for runaway electrons from thunderstorms. *Journal of Geophysical Research: Atmospheres*, *130*(10), e2024JD042350. https://doi.org/10.1029/2024JD042350

Eack, K. B., & Beasley, W. H. (2015). Long-duration x-ray emissions observed in thunderstorms. *Journal of Geophysical Research: Atmospheres*, *120*(14), 6887–6897. https://doi.org/10.1002/2015JD023262

Gurevich, G., Milikh, R., & Roussel-Dupre, R. (1992). Runaway electron mechanism of air breakdown and preconditioning during a thunderstorm. *Physics Letters A*, *165*(5), 463–468. https://doi.org/10.1016/0375-9601(92)90348-p

Heck, D., Knapp, J., Capdevielle, J. N., Schatz, G., & Thouw, T. (1998). Report No. FZKA 6019, 1998. https://www.ikp.kit.edu/corsika/70.php

Kelley, N. A., Smith, D. M., Dwyer, J. R., Splitt, M., Lazarus, S., Martinez-McKinney, F., et al. (2015). Relativistic electron avalanches as a thunderstorm discharge competing with lightning. *Nature Communications*, *6*(7845), 7845. https://doi.org/10.1038/ncomms8845

Marisaldi, M., Østgaard, N., Mezentsev, A., Lang, T., Grove, J. E., Shy, D., et al. (2024). Highly dynamic gamma-ray emissions are common in tropical thunderclouds. *Nature*, *634*(8032), 57–60. https://doi.org/10.1038/s41586-024-07936-6

Ostgaard, N., Christian, H. J., Grove, J. E., Sarria, D., Mezentsev, A., Kochkin, P., et al. (2019). Gamma-ray glow observations at 20-km altitude. *Journal of Geophysical Research: Atmospheres*, *124*(13), 7236–7254. https://doi.org/10.1029/2019JD030312

Sato, T. (2016). Analytical model for estimating the zenith angle dependence of terrestrial cosmic ray fluxes. *PLoS One*, *11*(8), e0160390. https://doi.org/10.1371/journal.pone.0160390

Stolzenburg, M., Marshall, T. C., Rust, W. D., et al. (2007). Electric field value observed near lightning flash initiations. *Geophysical Research Letters*, *34*, L04804. https://doi.org/10.1029/2006GL028777

Stolzenburg, M., Marshall, T. C., Rust, W. D., & Smull, B. F. (1994). Horizontal distribution of electrical and meteorological conditions across the stratiform region of a mesoscale convective system. *Monthly Weather Review*, *122*(8), 1777–1797. https://doi.org/10.1175/1520-0493(1994)122<1777:HDOEAM>2.0.co;2

Tsuchiya, H., Enoto, T., Yamada, S., Yuasa, T., Kawaharada, M., Kitaguchi, T., et al. (2007). Detection of high-energy gamma rays from winter thunderclouds. *Physical Review Letters*, *99*(16), 165002. https://doi.org/10.1103/PhysRevLett.99.165002

Wada, Y., Matsumoto, T., Enoto, T., Nakazawa, K., Yuasa, T., Furuta, Y., et al. (2021). Catalog of gamma-ray glow during four winter seasons in Japan. *Physical Review Research*, *3*(4), 043117. https://doi.org/10.1103/PhysRevResearch.3.043117